



HAL
open science

Hermite interpolation by planar cubic-like ATPH

Thierry Bay, Isabelle Cattiaux-Huillard, Laura Saini

► **To cite this version:**

Thierry Bay, Isabelle Cattiaux-Huillard, Laura Saini. Hermite interpolation by planar cubic-like ATPH. *Advances in Computational Mathematics*, 2022, 48, 10.1007/s10444-022-09978-8. hal-03556981v2

HAL Id: hal-03556981

<https://uphf.hal.science/hal-03556981v2>

Submitted on 24 Mar 2023

HAL is a multi-disciplinary open access archive for the deposit and dissemination of scientific research documents, whether they are published or not. The documents may come from teaching and research institutions in France or abroad, or from public or private research centers.

L'archive ouverte pluridisciplinaire **HAL**, est destinée au dépôt et à la diffusion de documents scientifiques de niveau recherche, publiés ou non, émanant des établissements d'enseignement et de recherche français ou étrangers, des laboratoires publics ou privés.

Hermite interpolation by planar cubic-like ATPH

Thierry Bay¹, Isabelle Cattiaux-Huillard¹, and Laura Saini²

¹Université Polytechnique Hauts-de-France, CERAMATHS, FR CNRS 2037, F-59313 Valenciennes, France - thierry.bay@uphf.fr, isabelle.cattiaux@uphf.fr

²Junia, Computer Science and Mathematics, F-59000 Lille, France - laura.saini@junia.com

March 4, 2023

Abstract

This paper deals with the construction of the Algebraic Trigonometric Pythagorean Hodograph (ATPH) cubic-like Hermite interpolant. A characterization of solutions according to the tangents at both ends and a global free shape parameter α is performed. Since this degree of freedom can be used for adjustments, we study how the curve evolves with respect to α . Several examples illustrating the construction process and a simple fitting method to determine the unique ATPH curve passing through a given point are proposed.

Keywords: Pythagorean hodograph · Trigonometric functions · Algebraic trigonometric · Trigonometric polynomials · Circle arc · Hermite interpolation

Mathematics Subject Classifications (2020): 41A05 · 42A15 · 51N05 · 65D05 · 65D07 · 65D10 · 65D17 · 68U07

1 Introduction

The most commonly used schemes in CAD and CAGD for the representation of curves and surfaces are specified by polynomial and rational parameterizations, such as Bézier curves, B-splines or NURBS. Even though these models offer many advantages, they have important drawbacks detailed in [14]. For example, on the one hand, polynomial Bézier curves are quite simple to define, compute and manipulate, but exclude important curve families as conics, cycloidal curves, etc. On the other hand, rational parameterization allows to obtain conics and trigonometric curves, but comes at the expense of additional weights for each control point and a heavy process for differentiation. Therefore, looking for an alternative representation is necessary. Moreover, obtaining both straight line segments and circle arcs in the same model is an undeniable advantage in environments associated with Computer Numerical Control Machines and for the conversion of trajectories into G-code. For this purpose, it could be interesting to investigate other curve spaces.

Responding to this problem, Carnicer and Peña [4] introduced the concept of B-basis to generalize the Bernstein bases for other function spaces, while Mainar et al. [14] provided criteria to find one in a general case. The underlying curves display all the positive properties of the Bézier scheme from variation diminishing property to tangency to the control polygon at

the endpoints. These authors gave a particular solution for the mixed Algebraic Trigonometric (AT) curve space $\mathcal{P}_m = \text{span}\{1, t, \{\cos(kt), \sin(kt)\}_{k=1}^m\}$ for $m = 1$ and $m = 2$. In these bases, the curves are described on $[0, \alpha]$ unlike the Bézier curves which are drawn on $[0, 1]$. The real $\alpha \in]0, 2\pi[$ can then be used as a shape parameter. An interactive illustration of the B-basis, the curves of \mathcal{P}_1 and the influence of α on the shape of the curve is available in [5].

The Pythagorean Hodograph (PH) polynomial curves, characterized by a polynomial parametric speed, was introduced in [11]. Combining this feature with the mixed AT space \mathcal{P}_m , a partial investigation of quintic-like Algebraic Trigonometric Pythagorean Hodograph curves (ATPH) is put forward for $m = 2$ in [18]. Generalizing from this concept, we gave in [6] a straightforward and exhaustive description of these curves through their complex expression and proposed an in-depth study of spaces \mathcal{P}_1 and \mathcal{P}_2 . In our paper, we focus on these \mathcal{P}_1 ATPH curves, so-called cubic-like ATPH, to solve the Hermite interpolation problem while taking into account the shape parameter of the B-basis.

Indeed, the existence of polynomial PH solutions of different forms of the Hermite problem was deeply investigated. A cubic solution for the G^1 planar case was proposed with one arc in [15, 3], bi-arc in [2] and as spline in [13, 23]. Spatial cubic interpolation was studied in [1]. Quintic PH interpolation was also the subject of many works concerning the planar (see [10, 16]) and the spatial case (see [21, 8, 9]). About the ATPH feature, only quintic solutions were considered for planar curves in [18] and for spatial curves in [17, 20]. But, according to our knowledge, cubic-like ATPH have never been applied to address the first-order Hermite interpolation problem. This article is then devoted to the study of such planar ATPH cubic-like curves, solutions of the G^1 Hermite interpolation problem. A focus is done on detailing the conditions of their existence and some of their properties.

The remainder of this paper is organized as follows. Section 2 recalls some basic facts concerning the mixed AT space and properties of ATPH curves. In Section 3, we start with the study of the construction of cubic-like ATPH Hermite interpolants. Then, we analyze in Section 4 the conditions required for the existence of such solutions. Consequently, in Section 5, we look at the influence of the free parameter α on the curve by working on the control polygon. In Section 6, we focus on a use of the shape parameter α to find the ATPH cubic-like Hermite interpolant that passes through one given additional point, which are illustrated in Section 7 by several examples.

2 Preliminaries

In [14], the authors proposed B-bases for several AT curve spaces. In particular, they described the normalized \mathcal{P}_1 B-basis (Z_0, Z_1, Z_2, Z_3) , depending on α belonging to the interval $]0, 2\pi[$ and for $t \in [0, \alpha]$ as:

$$\begin{aligned} Z_3(t) &= \frac{t - \sin t}{S_\alpha}, & Z_0(t) &= Z_3(\alpha - t), \\ Z_2(t) &= M_\alpha \left(\frac{1 - \cos t}{C_\alpha} - Z_3(t) \right), & Z_1(t) &= Z_2(\alpha - t), \end{aligned} \tag{1}$$

where $S_\alpha = \alpha - \sin \alpha$, $C_\alpha = 1 - \cos \alpha$, $R_\alpha = 2 \sin \alpha - \alpha - \alpha \cos \alpha$ and $M_\alpha = \frac{C_\alpha \sin \alpha}{R_\alpha}$ if $\alpha \neq \pi$, $M_\pi = 1$ otherwise. This formulation is short and elegant but not suitable to perform a change of basis between the canonical basis and the B-basis. So, in [6], we proposed a detailed expression of the matricial form.

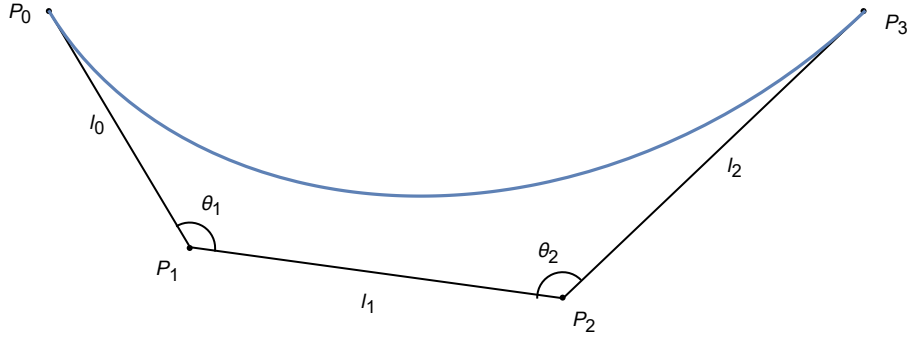


Figure 1: Cubic-like ATPH polygon data.

In this basis, a curve parameterization $\mathbf{R}_\alpha(t)$ of \mathcal{P}_1 is described by four control points \mathbf{P}_0 , \mathbf{P}_1 , \mathbf{P}_2 and \mathbf{P}_3 . This representation admits a complex interpretation, which is especially efficient to characterize PH curves, as proved by Farouki in [7] for the polynomial case. We extended this result to the ATPH curves in [6]. Denoting by $\mathbf{r}_\alpha(t)$, \mathbf{p}_0 , \mathbf{p}_1 , \mathbf{p}_2 and \mathbf{p}_3 the complex forms of $\mathbf{R}_\alpha(t)$ and its control points¹, its complex expression is

$$\mathbf{r}_\alpha(t) = \sum_{k=0}^3 \mathbf{p}_k Z_k(t). \quad (2)$$

A cubic-like ATPH curve is characterized by the complex relation:

$$(\Delta \mathbf{p}_1)^2 = K_\alpha \Delta \mathbf{p}_0 \Delta \mathbf{p}_2 \quad \text{with} \quad K_\alpha = \frac{4}{(\alpha - \sin \alpha)^2} \left(2 \sin \frac{\alpha}{2} - \alpha \cos \frac{\alpha}{2} \right)^2, \quad (3)$$

where $\Delta \mathbf{p}_k = \mathbf{p}_{k+1} - \mathbf{p}_k$. This condition can be geometrically rewritten by:

$$l_1^2 = K_\alpha l_0 l_2 \quad \text{and} \quad \theta_1 = \theta_2, \quad (4)$$

where $\theta_1 = \angle(\mathbf{P}_0 - \mathbf{P}_1, \mathbf{P}_2 - \mathbf{P}_1)$, $\theta_2 = \angle(\mathbf{P}_1 - \mathbf{P}_2, \mathbf{P}_3 - \mathbf{P}_2)$ and, in polar form, $\Delta \mathbf{p}_k = l_k e^{i\beta_k}$ for $k = 0, 1, 2$ (cf. Figure 1).

Afterwards, the K_α value appears many times. It is therefore necessary to detail its elementary properties that can be established by some straightforward calculations.

Proposition 1. *The term K_α is an increasing and continuous function of α . It belongs to the range $]1, 4[$ when α is in the interval $]0, 2\pi[$ and K_α tends to 1 as α approaches 0. Moreover*

$$\sqrt{K_\alpha} = \frac{2}{\alpha - \sin \alpha} \left(2 \sin \frac{\alpha}{2} - \alpha \cos \frac{\alpha}{2} \right).$$

The values $\alpha = 0$ and $\alpha = 2\pi$ are excluded from our study. On one hand, when α approaches 0, the cubic-like AT curve becomes the cubic polynomial Bézier curve of the same control polygon as shown by Zhang in [22]. This is consistent with the formula (3) and (4), since when $K_\alpha = 1$, these expressions are identical to the homologous relations given by Farouki in [7].

On the other hand, the second and third functions $Z_1(t)$ and $Z_2(t)$ of the B-basis vanish as $\alpha = 2\pi$. Therefore the curve parameterized by $\mathbf{r}_\alpha(t)$, with $t \in [0, \alpha]$, tends to the segment $[\mathbf{P}_0 \mathbf{P}_3]$, which obviously constitutes an improper solution.

¹In the following, notations in bold upper case will refer to points, and those in bold lower case to their complex form.

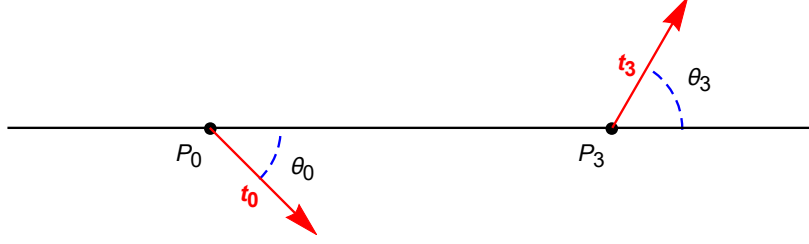


Figure 2: G^1 Hermite interpolation data.

3 Cubic-like ATPH solutions for the Hermite problem

The Hermite problem we are going to deal with consists of interpolating two points and two tangent directions by a cubic-like ATPH curve. Therefore, we consider two distinct points \mathbf{P}_0 and \mathbf{P}_3 and two oriented angles, $\theta_0 \in [-\pi, 0]$ and $\theta_3 \in [0, 2\pi[$. The choice of these intervals allows us to study all possible cases without any loss of generality.

In the coordinate system $(\mathbf{P}_0, \mathbf{i}, \mathbf{j})$ where $\mathbf{i} = \frac{\mathbf{P}_3 - \mathbf{P}_0}{\|\mathbf{P}_3 - \mathbf{P}_0\|}$ and $\mathbf{j} = \text{rot}_{\frac{\pi}{2}}(\mathbf{i})$, we define two unit tangent vectors $\mathbf{t}_0 = (\cos \theta_0, \sin \theta_0)$ and $\mathbf{t}_3 = (\cos \theta_3, \sin \theta_3)$ (cf. Figure 2). We need to verify:

$$\begin{aligned} \mathbf{R}_\alpha(0) &= \mathbf{P}_0, & \mathbf{R}_\alpha(\alpha) &= \mathbf{P}_3, \\ \frac{d\mathbf{R}_\alpha}{dt}(0) &= \lambda_0 \mathbf{t}_0, & \frac{d\mathbf{R}_\alpha}{dt}(\alpha) &= \lambda_3 \mathbf{t}_3, \end{aligned}$$

where λ_0 and λ_3 are strictly positive real numbers. Note that if \mathbf{t}_0 and \mathbf{t}_3 are both colinear with $\mathbf{P}_3 - \mathbf{P}_0$, the solution of Hermite's problem is trivially a line segment and is of little interest. Therefore, we will exclude this case in the rest of the article, and we will denote by \mathcal{H} the domain $[-\pi, 0] \times [0, 2\pi[$ for (θ_0, θ_3) without couples $(-\pi, 0)$, $(-\pi, \pi)$, $(0, 0)$ and $(0, \pi)$.

From the data described above, we have $\theta_1 = \pi - \beta_0 + \beta_1$ and $\theta_2 = \pi - \beta_1 + \beta_2$. Besides, the G^1 Hermite conditions imply $\beta_0 = \theta_0$ and $\beta_2 = \theta_3$. From (4), we therefore deduce $-\beta_0 + \beta_1 = -\beta_1 + \beta_2$, hence $\beta_1 = \frac{1}{2}(\beta_0 + \beta_2)$ to within π . So

$$\beta_1 = \frac{1}{2}(\theta_0 + \theta_3) \quad \text{or} \quad \beta_1 = \frac{1}{2}(\theta_0 + \theta_3) + \pi. \quad (5)$$

To begin with, let us consider the first possibility. Afterwards, we will see how to take into account the second one. It is clear that:

$$\begin{aligned} \Delta \mathbf{p}_0 + \Delta \mathbf{p}_1 + \Delta \mathbf{p}_2 &= \mathbf{p}_3 - \mathbf{p}_0, \\ l_0 e^{i\beta_0} + l_1 e^{i\beta_1} + l_2 e^{i\beta_2} &= \mathbf{p}_3 - \mathbf{p}_0, \\ l_0 e^{i\theta_0} + \sqrt{K_\alpha l_0 l_2} e^{i\frac{\theta_0 + \theta_3}{2}} + l_2 e^{i\theta_3} &= \mathbf{p}_3 - \mathbf{p}_0, \end{aligned} \quad (6)$$

so, if we set $L = \sqrt{\frac{l_2}{l_0}}$,

$$(3) \Leftrightarrow e^{i\theta_0} + L\sqrt{K_\alpha} e^{i\frac{\theta_0 + \theta_3}{2}} + L^2 e^{i\theta_3} = \frac{\mathbf{P}_3 - \mathbf{P}_0}{l_0}, \quad (7)$$

$$\Im(7) \Leftrightarrow \sin \theta_0 + L\sqrt{K_\alpha} \sin\left(\frac{\theta_0 + \theta_3}{2}\right) + L^2 \sin \theta_3 = 0, \quad (8)$$

$$\Re(7) \Leftrightarrow \cos \theta_0 + L\sqrt{K_\alpha} \cos\left(\frac{\theta_0 + \theta_3}{2}\right) + L^2 \cos \theta_3 = \frac{\|\mathbf{P}_3 - \mathbf{P}_0\|}{l_0}. \quad (9)$$

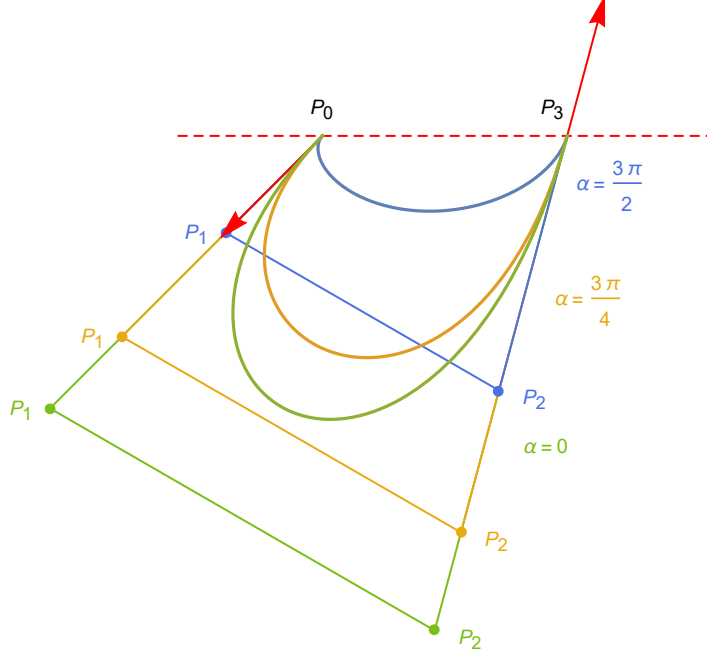


Figure 3: Solutions for $\alpha = 0$ (polynomial case), $\alpha = \frac{3\pi}{4}$ and $\alpha = \frac{3\pi}{2}$.

When the degree of equation (8) is 2 with respect to L , i.e. for $\theta_3 \neq 0$ and $\theta_3 \neq \pi$, the discriminant is

$$\Delta = K_\alpha \sin^2 \left(\frac{\theta_0 + \theta_3}{2} \right) - 4 \sin \theta_0 \sin \theta_3, \quad (10)$$

and the solutions, when they exist, are

$$L_\varepsilon = \frac{1}{2 \sin \theta_3} \left(-\sqrt{K_\alpha} \sin \left(\frac{\theta_0 + \theta_3}{2} \right) + \varepsilon \sqrt{\Delta} \right), \quad (11)$$

where $\varepsilon \in \{-1, +1\}$. For the sake of clarity, we will denote them respectively L_- and L_+ . When the real number

$$G_\varepsilon = \cos \theta_0 + L_\varepsilon \sqrt{K_\alpha} \cos \left(\frac{\theta_0 + \theta_3}{2} \right) + L_\varepsilon^2 \cos \theta_3 \quad (12)$$

is positive, we deduce from (9) the value of l_0 and then l_2 . With the previous expressions of β_0 , β_1 and β_2 , we can determine $\Delta \mathbf{p}_i$, for $i = 0, 1, 2$ and therefore the control polygon of the solution \mathbf{r}_α .

When $\theta_3 = 0$ or $\theta_3 = \pi$, equation (8) is of degree 1 with respect to L and requires a specific study which is done in Section 4.4.

From these results, we can easily notice that the ATPH provides an infinite number of solutions - depending on α - for a given initial data set. In Part 2, we put forward that the polynomial cubic PH curve can be seen as a particular case of cubic-like ATPH, obtained for $\alpha = 0$ and $K_\alpha = 1$. This is consistent with our results, since when $K_\alpha = 1$, the expressions (10), (11) and (12) are identical to the formulas given by Walton and Meek in [15] and by Byrtus and Bastl in [3] for the polynomial case. The Figure 3 shows two ATPH solutions and their polynomial equivalent.

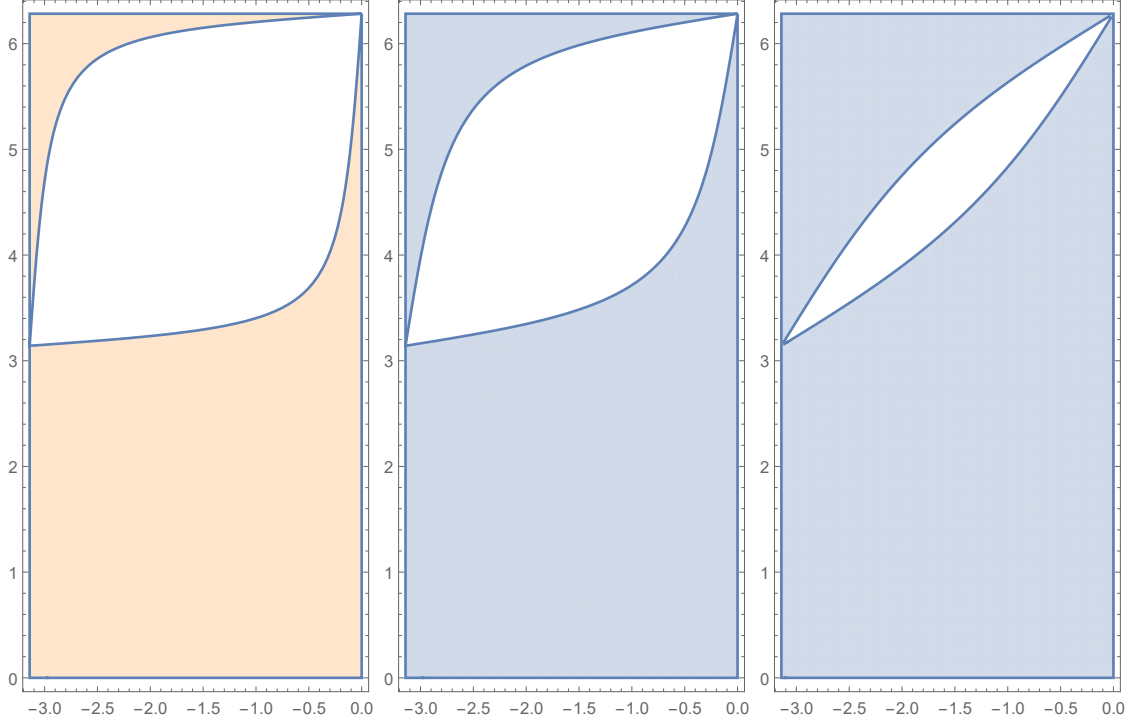


Figure 4: Domain \mathcal{D}_+ for $\alpha = 0$ (polynomial case), $\alpha = \frac{7\pi}{6}$ and $\alpha = \frac{11\pi}{6}$.

4 Existence of solutions

The solutions described in the previous part do not always exist. We now have to clarify their conditions of existence, i.e. the domains on which the values of Δ , G_ε , L_ε , defined by the expressions (10), (11), (12) are positive. As said previously, the cases $\theta_3 = 0$ and $\theta_3 = \pi$ are different from the general one and will be treated separately.

4.1 Sign of the discriminant

Let us denote by \mathcal{D}_+ the domain of \mathcal{H} where $\Delta \geq 0$, whose boundary is defined by the functions:

$$f_1(\theta_0) = 2\pi - \arccos \frac{K_\alpha^2 \cos \theta_0 - 4(8 - K_\alpha)\sqrt{4 - K_\alpha} \sin^2 \theta_0}{K_\alpha^2 + 16(4 - K_\alpha) \sin^2 \theta_0},$$

$$f_2(\theta_0) = 2\pi - \arccos \frac{K_\alpha^2 \cos \theta_0 + 4(8 - K_\alpha)\sqrt{4 - K_\alpha} \sin^2 \theta_0}{K_\alpha^2 + 16(4 - K_\alpha) \sin^2 \theta_0}.$$

Since $K_\alpha \in]1, 4[$, these two functions are well defined for any value of $\alpha \in]0, 2\pi[$. Of course, the shape of this domain depends on this last parameter (see Figure 4). The function f_1 describes the lower border of the domain, and f_2 the upper border (see Figure 5). So the domain \mathcal{D}_+ is described by

$$\mathcal{D}_+ = \{(\theta_0, \theta_3) \in \mathcal{H} \mid \theta_3 \leq f_1(\theta_0) \text{ or } f_2(\theta_0) \leq \theta_3\}.$$

We can remark that for $\theta_3 < \pi$, we have $\Delta > 0$, hence the condition is always verified.

4.2 Sign of l_0

Once L_ε is determined using (11), l_0 is obtained from the relation (9). Therefore, l_0 and the real number G_ε have the same sign which has to be positive. Moreover, the case $G_\varepsilon = 0$ should be excluded, otherwise the length l_0 would be infinite. Here we will study the sign of G_ε , as defined in (12), using the expression (11) for L_ε .

Denoting Γ_+ and Γ_- the subdomains of \mathcal{H} where $G_+ > 0$ and $G_- > 0$ respectively, a solution exists if and only if (θ_0, θ_3) belongs to $\Gamma = \Gamma_+ \cup \Gamma_-$. The relations (11) and (12) allow us to establish that

$$4G_\varepsilon \sin^2 \theta_3 = A + B, \quad (13)$$

where:

$$\begin{aligned} A &= 2 \sin \left(\frac{\theta_3 - \theta_0}{2} \right) \left(4 \sin \theta_3 \cos \left(\frac{\theta_3 - \theta_0}{2} \right) - K_\alpha \sin \left(\frac{\theta_0 + \theta_3}{2} \right) \right), \\ B &= 2\varepsilon \sqrt{K_\alpha} \sin \left(\frac{\theta_3 - \theta_0}{2} \right) \sqrt{\Delta}. \end{aligned}$$

Then, we have $G_\varepsilon = 0$ if and only if $\sin \left(\frac{\theta_3 - \theta_0}{2} \right) = 0$ or $A' - B' = 0$, with:

$$\begin{aligned} A' &= 4 \sin \theta_3 \cos \left(\frac{\theta_3 - \theta_0}{2} \right) - K_\alpha \sin \left(\frac{\theta_0 + \theta_3}{2} \right), \\ B' &= \varepsilon \sqrt{K_\alpha} \sqrt{\Delta}. \end{aligned}$$

Evidently, the former equation has for solution $\theta_3 = \theta_0 + 2\pi$ in \mathcal{H} , which leads to $\Delta < 0$. From the latter one, we obtain:

$$A'^2 - B'^2 = 4(2 + 2 \cos(\theta_3 - \theta_0) - K_\alpha) \sin^2 \theta_3. \quad (14)$$

The sign of this expression changes for $\theta_3 = \psi_k(\theta_0)$ or $\theta_3 = \overline{\psi}_k(\theta_0)$ where:

$$\psi_k(\theta_0) = \theta_0 + \arccos \left(\frac{K_\alpha}{2} - 1 \right) + 2k\pi, \quad (15)$$

$$\overline{\psi}_k(\theta_0) = \theta_0 - \arccos \left(\frac{K_\alpha}{2} - 1 \right) + 2k\pi. \quad (16)$$

Since $K_\alpha \in]1, 4[$ according to Proposition 1, these functions are well defined. Only the lines corresponding to $\psi_0(\theta_0)$, $\psi_1(\theta_0)$ and $\overline{\psi}_1(\theta_0)$ are in the domain \mathcal{H} (cf. Figure 5) and are involved in the description of Γ_+ and Γ_- (cf. Figures 6 and 7). These domains are formally described by:

$$\begin{aligned} \Gamma_+ &= \{(\theta_0, \theta_3) \in \mathcal{H} \mid \theta_3 \geq \pi - \theta_0 \text{ and } (f_2(\theta_0) < \theta_3 < \psi_1(\theta_0) \text{ or } \theta_3 < f_1(\theta_0))\} \\ &\quad \cup \{(\theta_0, \theta_3) \in \mathcal{H} \mid \theta_3 < \pi - \theta_0 \text{ and } (\theta_3 < \overline{\psi}_1(\theta_0))\}, \\ \Gamma_- &= \{(\theta_0, \theta_3) \in \mathcal{H} \mid \theta_3 \geq \pi - \theta_0 \text{ and } (f_2(\theta_0) < \theta_3 \text{ or } \overline{\psi}_1(\theta_0) < \theta_3 < f_1(\theta_0))\} \\ &\quad \cup \{(\theta_0, \theta_3) \in \mathcal{H} \mid \theta_3 < \pi - \theta_0 \text{ and } (\theta_3 < \psi_0(\theta_0) \text{ or } \psi_1(\theta_0) < \theta_3)\}. \end{aligned}$$

This result is a generalization of [3] focusing on the polynomial curves, which corresponds to the case $K_\alpha = 1$ for $\alpha = 0$ in our study. The ATPH feature provides therefore a wider domain of solutions through the variations induced by the α parameter.

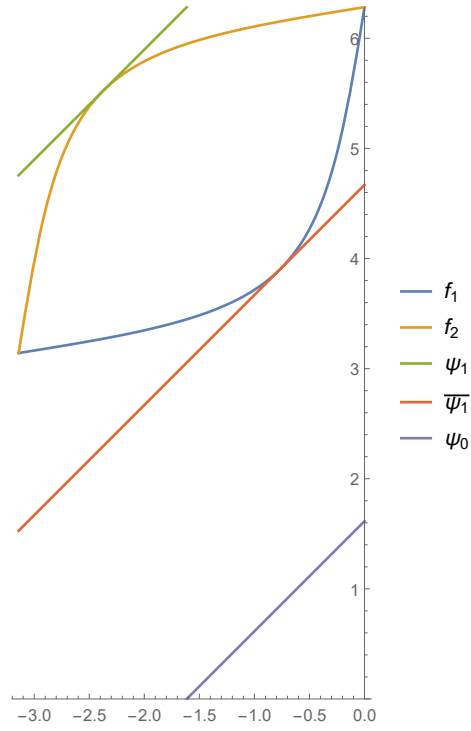


Figure 5: Edges of \mathcal{D}_+ , Γ_+ and Γ_- domains for $\alpha = \frac{7\pi}{6}$.

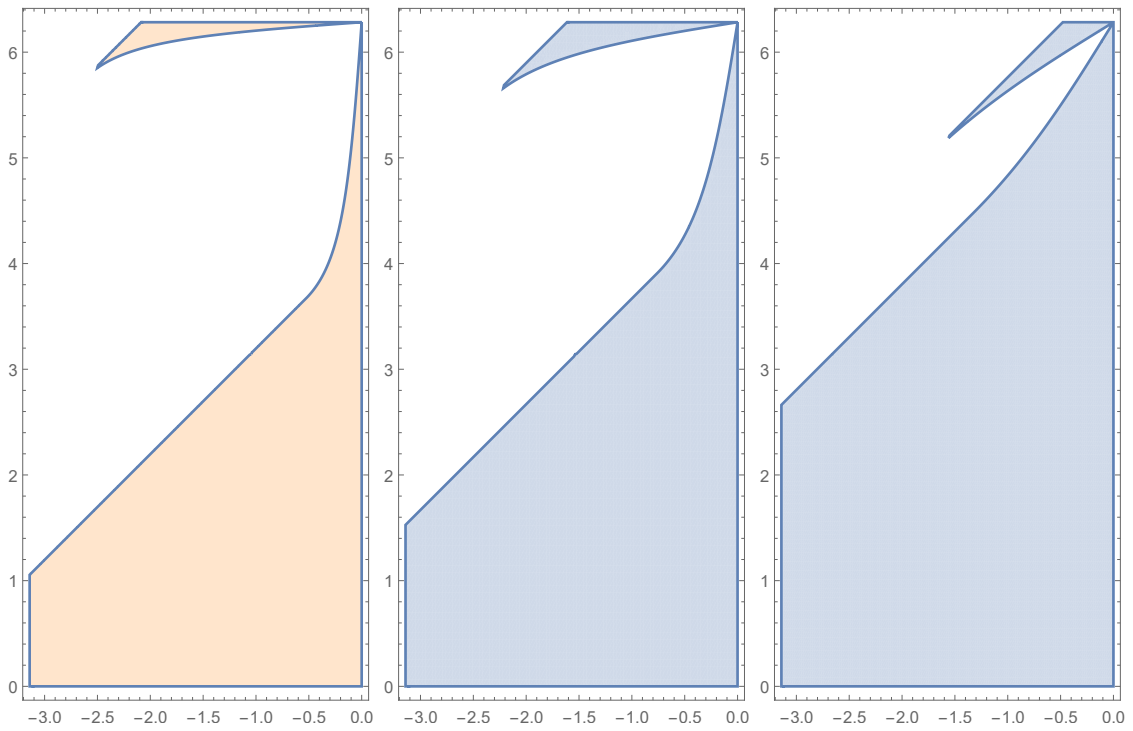


Figure 6: Subdomain Γ_+ for $\alpha = 0$ (polynomial case), $\alpha = \frac{7\pi}{6}$ and $\alpha = \frac{11\pi}{6}$.

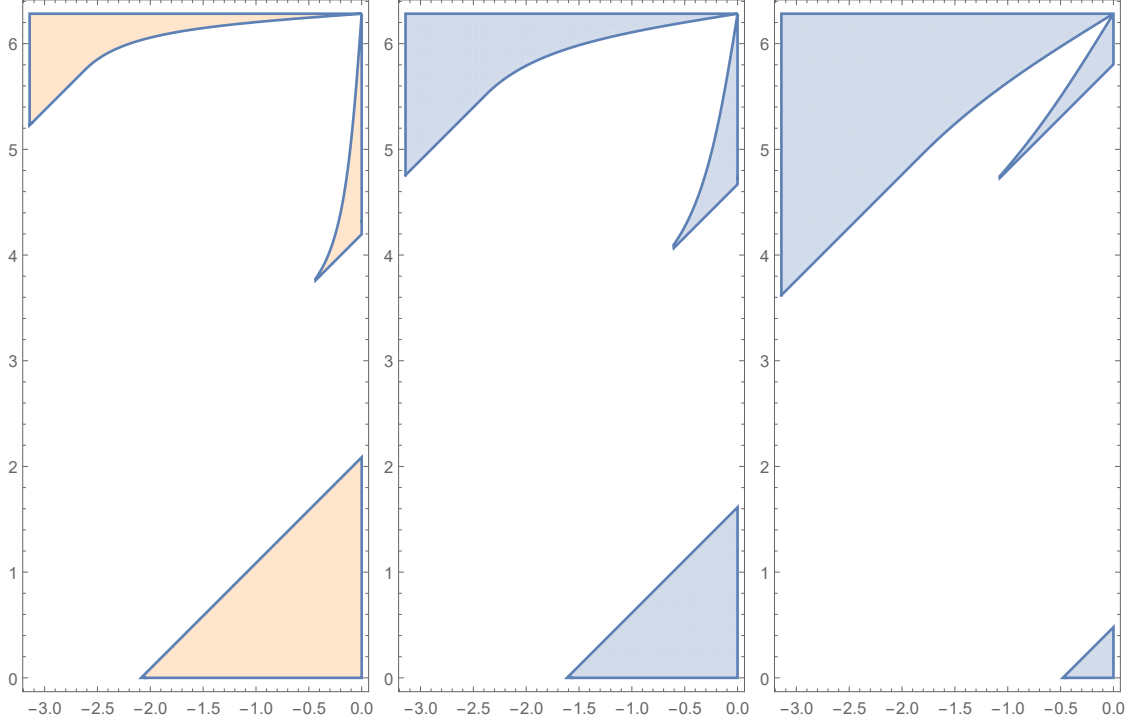


Figure 7: Subdomain Γ_- for $\alpha = 0$ (polynomial case), $\alpha = \frac{7\pi}{6}$ and $\alpha = \frac{11\pi}{6}$.

Remark 1. If $\Delta \geq 0$ and $G_\varepsilon < 0$, the curve exists with $l_0 < 0$ and therefore $l_2 < 0$. A length being positive, the notion of algebraic measure would then be more appropriate to cover this case. As seen in Figure 8, this means geometrically that the orientations of vectors $\mathbf{P}_1 - \mathbf{P}_0$ and \mathbf{t}_0 are opposite, as the orientations of $\mathbf{P}_3 - \mathbf{P}_2$ and \mathbf{t}_3 are. If the constraints of the Hermite problem concern only the direction of the tangents and not their orientation, these solutions are convenient. The only condition that θ_0 and θ_3 must then verify is $\Delta \geq 0$, ie $(\theta_0, \theta_3) \in \mathcal{D}_+$.

4.3 Sign of roots

As $L_\varepsilon = \sqrt{l_2/l_0}$, its value is positive. However, equation (8) can have negative roots. We will show that they are also solutions of the Hermite problem.

Relation (5) gives two expressions for β_1 . The second one leads to slightly different expressions of equations (8) and (9):

$$\sin \theta_0 - L\sqrt{K_\alpha} \sin \left(\frac{\theta_0 + \theta_3}{2} \right) + L^2 \sin \theta_3 = 0, \quad (17)$$

$$\cos \theta_0 - L\sqrt{K_\alpha} \cos \left(\frac{\theta_0 + \theta_3}{2} \right) + L^2 \cos \theta_3 = \frac{\|\mathbf{P}_3 - \mathbf{P}_0\|}{l_0}. \quad (18)$$

Expression (18) being the value of G_ε , we notice that L_ε is a solution of (8) if and only if $-L_\varepsilon$ is a solution of (17). Therefore, the solution $-L_\varepsilon$ of (17) is identical to the expression given by (9) for L_ε . So the value of l_0 is the same in both cases.

Proposition 2. When $L_\varepsilon < 0$, we still have $l_0 = \frac{\|\mathbf{P}_3 - \mathbf{P}_0\|}{G_\varepsilon}$ and $l_2 = L_\varepsilon^2 l_0$. In this case, $\beta_1 = \pi + \frac{\theta_0 + \theta_3}{2}$ and the polygon $(\mathbf{P}_0, \mathbf{P}_1, \mathbf{P}_2, \mathbf{P}_3)$ is then crossed (see Figure 9).

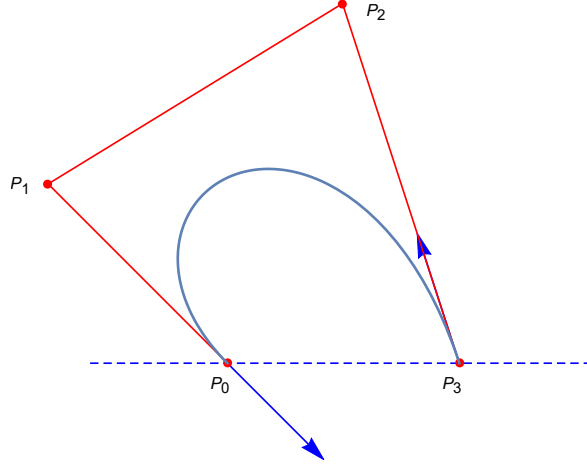


Figure 8: Improper solution when G_ε is negative, for $\alpha = \frac{2\pi}{3}$, $\theta_0 = -\frac{\pi}{4}$ and $\theta_3 = \frac{3\pi}{5}$.

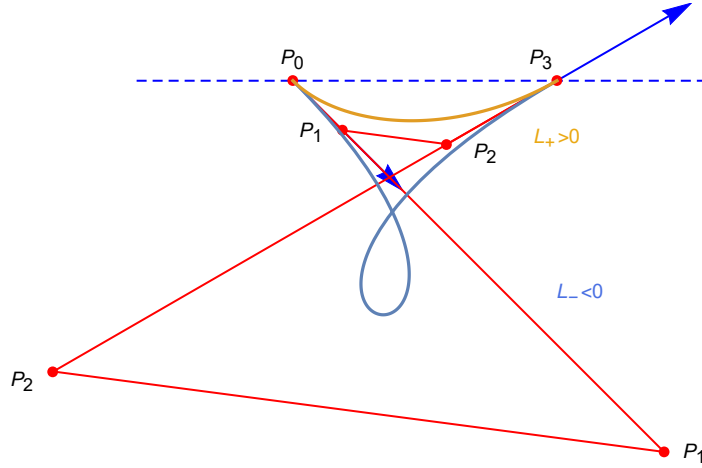


Figure 9: Example of a double solution with $L_+ > 0$ and $L_- < 0$.

A crossed polygon often gives a looped curve, which is rarely suitable in CAGD. As a consequence, it is important to determine the sign of L_ε when $G_\varepsilon > 0$ and $\Delta \geq 0$. Some considerations about the roots of equation (8) lead to the following result.

Proposition 3. *When the roots of equation (8) exist and verify $G_\varepsilon > 0$, we have $L_+ > 0$ for all the values of θ_0 and θ_3 , and $L_- > 0$ if and only if $\theta_3 > \pi$. The polygon is then crossed if and only if $\varepsilon = -1$ and $\theta_3 < \pi$.*

4.4 Particular case: $\theta_3 = 0$ and $\theta_3 = \pi$

As said in Section 3, equation (8) is of degree 1 when $\theta_3 = 0$ or $\theta_3 = \pi$.

If $\theta_3 = 0$, its solution is then $L = L_0 = \frac{-2}{\sqrt{K_\alpha}} \cos \frac{\theta_0}{2}$ which is always negative. So $\beta_1 = \pi + \frac{\theta_0 + \theta_3}{2}$ (according to Proposition 2) and its polygon is Z-shaped. Denoting G_0 the equivalent

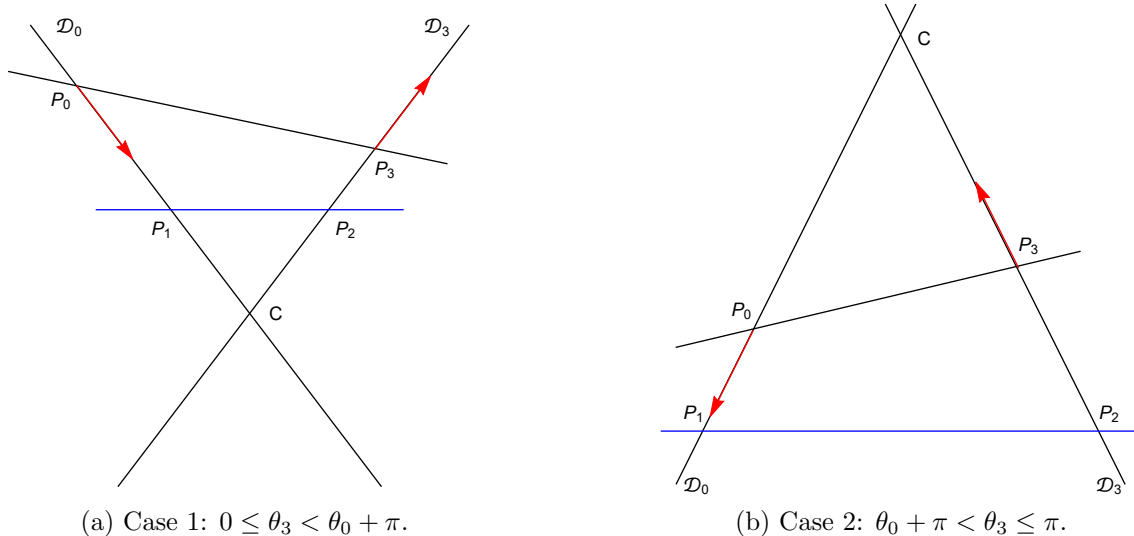


Figure 10: Shape of the control polygon when the lines \mathcal{D}_0 and \mathcal{D}_3 intersect.

of G_ε for L_0 , we obtain from (18) $G_0 = 1 + \frac{2}{K_\alpha} + 2 \left(1 + \frac{1}{K_\alpha}\right) \cos \theta_0$ which is positive if and only if $\theta_0 > \arccos \left(\frac{K_\alpha + 2}{2(K_\alpha + 1)} \right) - \pi$.

If $\theta_3 = \pi$, the solution of equation (8) is $L = L_\pi = \frac{-2}{\sqrt{K_\alpha}} \sin \frac{\theta_0}{2}$ which is positive. With the same convention, $G_\pi = \frac{1}{K_\alpha} (2 \cos \theta_0 - 2 + K_\alpha)$ is positive if and only if $\theta_0 > -\arccos \left(1 - \frac{K_\alpha}{2} \right)$.

5 Evolution of the solution polygon with respect to α

The shape of the control polygon determines the curve and may sometimes involve the presence of inflection points, cusps or loops. As said previously, these elements are undesirable for most CAD, CAD/CAM, or computer graphics applications. A sufficient condition to eliminate undesired elements according to the variation diminishing property is to consider convex polygons. We then focus the rest of this paper on this case. Obviously, this requirement is equivalent to $\theta_3 < \pi$ and $\varepsilon = 1$. The corresponding two cases are illustrated in Figure 10.

The ATPH solution of the Hermite problem depends on α which gives an additional degree of freedom, the polynomial solution being a particular case obtained for $\alpha = 0$. This free parameter can be used to solve various additional problems (velocity, interpolation point, ...), as will be shown in Section 6. It is therefore important to analyze the evolution of the curve with respect to α . For this purpose, we will study a geometrical version of our problem through the different configurations of the control polygon.

Considering two points \mathbf{A} and \mathbf{B} , we denote by $\overline{\mathbf{AB}}$ the algebraic measure from \mathbf{A} to \mathbf{B} . Let \mathcal{D}_0 (resp. \mathcal{D}_3) be the line passing through \mathbf{P}_0 (resp. \mathbf{P}_3) with \mathbf{t}_0 (resp. \mathbf{t}_3) as orientation vector. Firstly, we suppose the existence of an intersection point of \mathcal{D}_0 and \mathcal{D}_3 , denoted by \mathbf{C} .

According to the initial constraints of the Hermite problem, the points \mathbf{P}_1 and \mathbf{P}_2 must be chosen such that $\mathbf{P}_1 - \mathbf{P}_0$ and \mathbf{t}_0 have the same orientation, and $\mathbf{P}_2 - \mathbf{P}_3$ and \mathbf{t}_3 are opposite vectors. The measures l_0 and l_2 are here defined algebraically with $l_0 = \overline{\mathbf{P}_0\mathbf{P}_1}$ and $l_2 = \overline{\mathbf{P}_2\mathbf{P}_3}$, which is consistent with the fact that these two values remain positive. Moreover, as $\theta_1 = \theta_2$

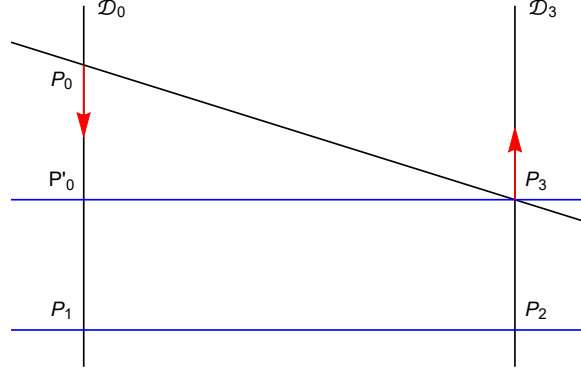


Figure 11: Shape of the control polygon when the lines \mathcal{D}_0 and \mathcal{D}_3 are parallel.

according to (4), the triangle $\mathbf{CP}_1\mathbf{P}_2$ is isosceles with apex \mathbf{C} . We therefore define the measures $a = \overline{\mathbf{CP}_0}$ and $b = \overline{\mathbf{CP}_3}$. These two values are constant with respect to α . As $\overline{\mathbf{CP}_1} = -\overline{\mathbf{CP}_2}$, we have $l_0 + a = l_2 - b$.

Moreover, the angles of $\mathbf{CP}_0\mathbf{P}_3$ being fixed with respect to α , there exists a constant value c such that $l_1 = \pm c(l_0 + a)$. From relation (4), we deduce a new expression of K_α as a function of l_0 , denoted by \tilde{K}_α and written as

$$\tilde{K}_\alpha(l_0) = \frac{c^2(l_0 + a)^2}{l_0(l_0 + a + b)}.$$

The derivative of this function with respect to l_0 is:

$$\frac{d\tilde{K}_\alpha}{dl_0} = -\frac{c^2(l_0 + a)}{l_0^2(l_0 + a + b)^2} (l_0(a - b) + a(a + b)).$$

To study the sign of this expression, we make the assumption $|a| > |b|$. As defined in Section 2, the B-basis (Z_0, Z_1, Z_2, Z_3) has the same property of symmetry as the Bernstein basis. So the case $|a| < |b|$ arises from the former one by considering the symmetrical problem with $\theta'_0 = -\theta_3$ and $\theta'_3 = -\theta_0$. The geometric constraints lead then to two distinct situations, as illustrated by Figure 10.

In the first case, we have $0 \leq \theta_3 < \theta_0 + \pi$, with $a < 0$ and $b > 0$. Since $l_0 < |a|$, $l_0 + a < 0$. Moreover, $l_0 + a = l_2 - b$ with $l_2 > 0$, so $l_0 + a + b > 0$. Finally, $l_0 > -(a + b) > 0$ and $a - b < a < 0$ lead to $l_0(a - b) + a(a + b) < 0$. The derivative is therefore negative. Similarly in the second case, when $\theta_0 + \pi < \theta_3 \leq \pi$, we have $a > 0$, $b < 0$ and $l_0 + a > 0$. As $a > -b$, we have $a + b > 0$ and $a - b > 0$, so $l_0(a - b) + a(a + b) > 0$. The derivative is negative again.

In the considered domain, the function \tilde{K}_α is a decreasing and continuous bijection with respect to l_0 . Moreover, the K_α form described in (3) is an increasing and continuous function of α (see Proposition 1). So $l_0 = \tilde{K}_\alpha^{-1}(K_\alpha)$ is continuous and decreasing with respect to α . The property is also true for l_2 , since $l_2 = l_0 + a + b$, the value $a + b$ being constant relatively to K_α .

Proposition 4. *When $\varepsilon = 1$, $\theta_3 < \pi$ and \mathcal{D}_0 and \mathcal{D}_3 intersect, the lengths l_0 and l_2 continuously decrease as α increases.*

When \mathcal{D}_0 and \mathcal{D}_3 are parallel, we have $\theta_3 = \theta_0 + \pi$, as illustrated by Figure 11. Indeed, for $\theta_3 = \theta_0 + 2\pi$, Δ is always negative and the interpolation problem has no solution. Let \mathbf{P}'_0 denote the projection of \mathbf{P}_3 onto \mathcal{D}_0 , along the line $(\mathbf{P}_1\mathbf{P}_2)$ and we suppose that $\mathbf{P}_0\mathbf{P}_1 > \mathbf{P}_2\mathbf{P}_3$

(the other case being symmetrical, as before). Let a and c be the distances $\mathbf{P}'_0\mathbf{P}_0$ and $\mathbf{P}'_0\mathbf{P}_3$ respectively. Here again, these two values are independent of the choice of α . As $\theta_1 = \theta_2$, the quadrilateral $\mathbf{P}'_0\mathbf{P}_1\mathbf{P}_2\mathbf{P}_3$ is then a rectangle and we have $l_2 = l_0 - a$ and $l_1 = c$. So according to equation (4), $c^2 = K_\alpha l_0(l_0 - a)$. Hence, we define

$$\tilde{K}_\alpha(l_0) = \frac{c^2}{l_0(l_0 - a)}.$$

Since $l_0 > a$, this function is obviously continuous and decreasing when $l_0 \in \mathbb{R}^+$. So, as for the intersecting case, we can establish the following result:

Proposition 5. *When $\varepsilon = 1$, $\theta_3 < \pi$ and \mathcal{D}_0 and \mathcal{D}_3 are parallel, the lengths l_0 and l_2 continuously decrease as α increases.*

Remark 2. *For $\varepsilon = 1$ and $\theta_3 < \pi$, the study points out that l_0 and l_2 also decrease as α increases. Though, for $\varepsilon = -1$ and $\theta_3 < \pi$, it can be proved that l_0 and l_2 are increasing functions with respect to α .*

6 Fitting method and unique interpolant

As a concrete example of use of the free parameter α in the Hermite interpolation, we propose an optimization process to determine its required value to satisfy an additional interpolation constraint. After determining the interval to which the α parameter should belong to get a solution, we infer the domain \mathcal{P} where the extra interpolation point \mathbf{D} has to be to ensure the existence of a solution. The fitting process is developed and illustrated via some examples.

6.1 The domain \mathcal{P}

According to Section 4, the required conditions for the existence of a solution are $\Delta > 0$ and $G_\varepsilon > 0$. These constraints modify the initial interval $]0, 2\pi[$ of α . For $\varepsilon = 1$ and $\theta_3 < \pi$, we can determine α_{min} and α_{max} , depending on θ_0 and θ_3 , such that the Hermite problem has a solution if and only if $\alpha \in]\alpha_{min}, \alpha_{max}[$.

On the studied domain, it can be easily proved that $\Delta > 0$. Therefore, the existence of a solution depends on the sign of G_+ . Indeed, according to Proposition 3, we have $L_+ > 0$ if $G_+ > 0$ without any condition on α . Moreover, the domain Γ_+ is bounded by the condition $\theta_3 < \overline{\psi}_1(\theta_0)$. If $\theta_3 < \theta_0 + \frac{4\pi}{3}$ this inequality is always true and $\alpha_{min} = 0$ (as $K_\alpha \in]1, 4[$ from Proposition 1). Otherwise, it is equivalent to $K_\alpha > 2 + 2\cos(\theta_3 - \theta_0)$ and α_{min} is the value for which

$$K_\alpha = 2 + 2\cos(\theta_3 - \theta_0). \quad (19)$$

This equation being transcendental, no closed-form solution exists and a numerical approximation is therefore necessary. As there is no upper bound for Γ_+ , we have evidently $\alpha_{max} = 2\pi$. The corresponding solution curve is then degenerated to the segment $[\mathbf{P}_0\mathbf{P}_3]$.

Properties 4 and 5 show that the lengths l_0 and l_2 continuously decrease as α increases. According to the variation diminishing property, the convex curve \mathbf{r}_α moves continuously from $\mathbf{r}_{\alpha_{min}}$ to $\mathbf{r}_{\alpha_{max}}$. The continuous curve \mathbf{r}_α then describes the area delimited by $\mathbf{r}_{\alpha_{min}}$ and $[\mathbf{P}_0\mathbf{P}_3]$, which is the domain \mathcal{P} we are looking for (see Figure 12). So, for any point \mathbf{D} in \mathcal{P} , there exists $\alpha_* \in]\alpha_{min}, \alpha_{max}[$ and $t_D \in [0, \alpha_*]$ such that $\mathbf{r}_{\alpha_*}(t_D) = \mathbf{D}$. This transcendental equation needs once again an algorithmic solving.

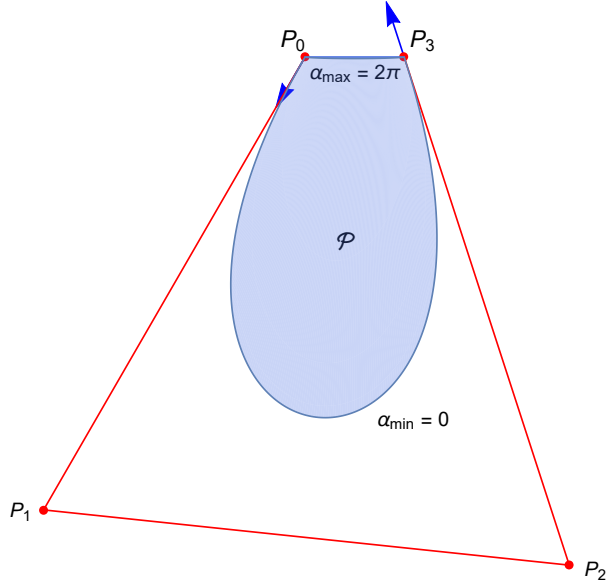


Figure 12: Domain \mathcal{P} for $\theta_0 = -\frac{2\pi}{3}$, $\theta_3 = \frac{3\pi}{5}$ and $\alpha_{min} = 0$.

Remark 3. When $\theta_3 > \theta_0 + \frac{4\pi}{3}$ and α_{min} is a solution of (19), we have $G_+ = 0$ implying that the length $l_0 = \frac{\|\mathbf{P}_3 - \mathbf{P}_0\|}{G_+}$ is theoretically infinite. Practically, even though the used value is an approximation, l_0 still increases dramatically with the accuracy of α_{min} . Even if it can be seen as an advantage since it involves a very large \mathcal{P} domain, it can lead to serious numerical instabilities when verifying the belonging of \mathbf{D} to \mathcal{P} and determining α_* . It is rather preferable to choose a value slightly greater than the solution of (19) for α_{min} .

6.2 The optimization process

The first question that must be answered is whether or not \mathbf{D} belongs to \mathcal{P} . It is done with a ray-tracing method [19, 12]. Let us consider the polygon resulting from a discretization of the curve $\mathbf{R}_{\alpha_{min}}$, that we have closed by joining the points \mathbf{P}_0 and \mathbf{P}_3 . The algorithm consists in casting a ray from \mathbf{D} and in counting the intersections of this ray with the edges of the polygon. If the number of intersections between the ray and each edge is even, the point \mathbf{D} is outside, otherwise \mathbf{D} is inside.

Once this step has been done, the fitting error defined by $E(\alpha) = \|\mathbf{D} - \mathbf{R}_\alpha(t_D)\|^2$ is minimized. The value $t_D \in [0, \alpha]$ is the parameter related to the closest orthogonal projection of \mathbf{D} onto \mathbf{R}_α (cf. Figure 13a). In other words, its value is obtained by determining the solution of

$$\mathbf{R}'_\alpha(t) \cdot (\mathbf{D} - \mathbf{R}_\alpha(t)) = 0 \quad (20)$$

that minimizes the distance between \mathbf{D} and $\mathbf{R}_\alpha(t)$.

Equation (20) being transcendental, an iterative Newton-Raphson-based approach is done to get t_D and then $E(\alpha)$. A dichotomy-based process is finally applied to minimize $E(\alpha)$ with respect to α (cf. Figure 13b). The reader can refer to Appendix A for further details about the algorithm behind the optimization process.

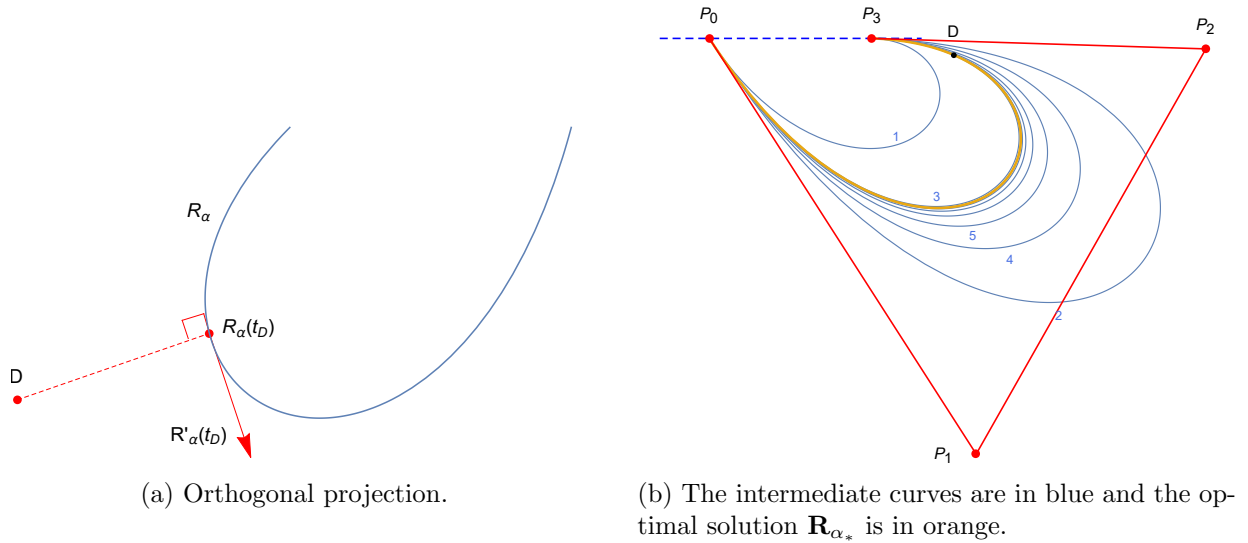


Figure 13: Fitting process with an interpolation point \mathbf{D} : orthogonal projection on the left and dichotomic fitting on the right.

7 Qualitative comparisons between PH and ATPH curves

In order to illustrate the contribution of ATPH, several examples comparing cubic-like ATPH and cubic PH solutions are detailed here. In each case, we interpolate a part of a classic curve. The control points \mathbf{P}_0 and \mathbf{P}_3 , as well as the angles θ_0 and θ_3 , are chosen from the parameterization of the reference curve.

7.1 Circle arcs

Since circle arcs are of major interest to the CAGD, the example of the circle is essential. In [6], we show that there is a cubic-like ATPH which represents it exactly, whatever the radius and the considered arc. Of course, this is not the case with PH curves. Not only does the PH Hermite interpolation only provides an approximation, but a solution also does not always exist.

Indeed, to interpolate a circle arc, the initial condition is $\theta_3 = -\theta_0 = \frac{1}{2}\alpha$ where α is the arc measure. The ATPH \mathbf{R}_α fits then exactly the circle arc without optimisation process. Denoting by \mathbf{R} the PH solution, it exists only if $\theta_3 < \theta_0 + \frac{4\pi}{3}$ (see [3]), i.e if $\theta_3 < \frac{2\pi}{3}$ or $\alpha < \frac{4\pi}{3}$. Moreover, when θ_3 approaches $\frac{2\pi}{3}$, l_0 tends to infinity and therefore the error diverges.

Let $E(\theta_3) = \|\mathbf{R}(\frac{1}{2}) - \mathbf{S}\|$ be the error, where \mathbf{S} is the apex of the circle arc (see Figure 14a) defined by

$$\mathbf{S} = \frac{1}{2}(\mathbf{P}_0 + \mathbf{P}_3) - \frac{\|\mathbf{P}_3 - \mathbf{P}_0\|}{2} \left(\frac{1}{\sin \theta_3} - \frac{1}{\tan \theta_3} \right) \cdot \mathbf{j}.$$

According to [15] for $\theta_3 = -\theta_0$, the PH solution of this Hermite problem verifies

$$l_0 = l_2 = \frac{\|\mathbf{P}_3 - \mathbf{P}_0\|}{1 + 2 \cos \theta_3}.$$

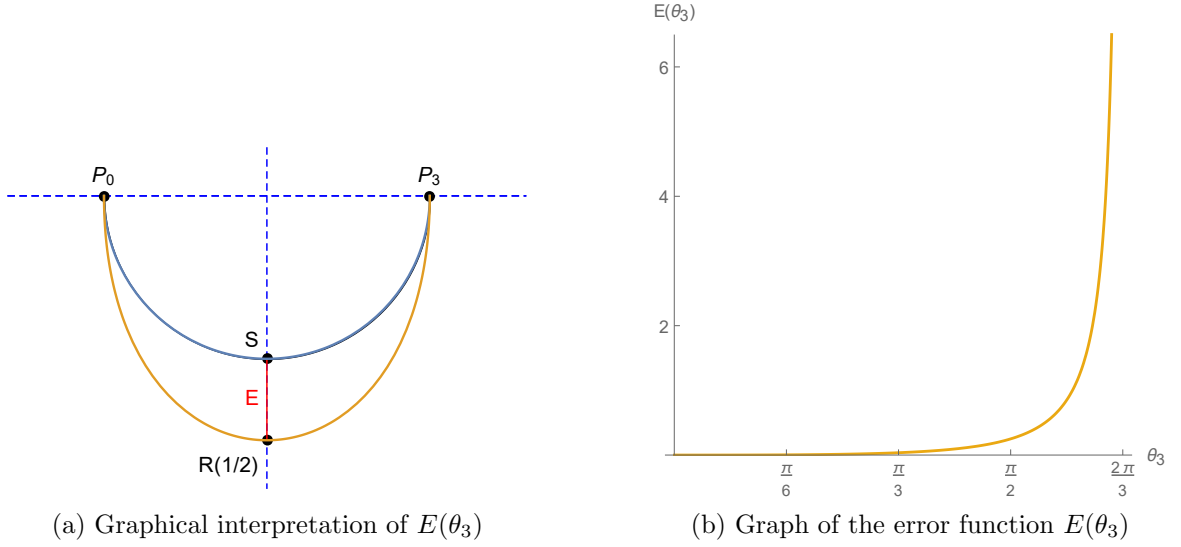


Figure 14: Error between ATPH circle arc (blue) and its PH approximation (orange).

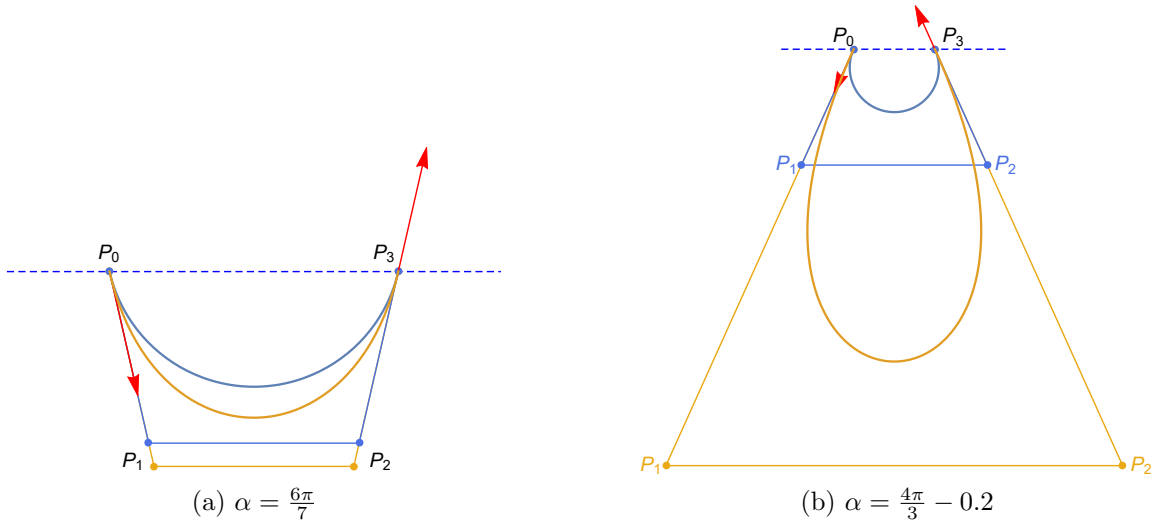


Figure 15: Reconstruction of a circle arc by ATPH (blue) and PH curves (orange).

Then, we have

$$\mathbf{R}\left(\frac{1}{2}\right) = \frac{1}{2}(\mathbf{P}_0 + \mathbf{P}_3) - \frac{3\|\mathbf{P}_3 - \mathbf{P}_0\|}{4(1 + 2\cos\theta_3)} \sin\theta_3 \cdot \mathbf{j}.$$

The error is

$$\begin{aligned} E(\theta_3) &= \frac{1}{\|\mathbf{P}_3 - \mathbf{P}_0\|} \left\| \mathbf{R}\left(\frac{1}{2}\right) - \mathbf{S} \right\| \\ &= \frac{3\sin\theta_3}{4(1 + 2\cos\theta_3)} - \frac{1}{2} \left(\frac{1}{\sin\theta_3} - \frac{1}{\tan\theta_3} \right). \end{aligned}$$

Its behavior is illustrated by Figure 14b, and Figure 15 illustrates the difference between the PH and ATPH solutions for two values of α .

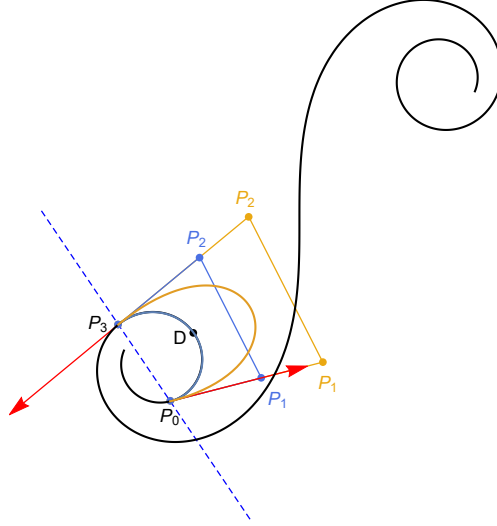


Figure 16: Interpolation of a clothoid arc with the PH (orange) and the ATPH curves (blue).

7.2 Clothoid

Let us consider the example of a clothoid, defined by the normalized Fresnel integrals

$$\mathbf{C}_1(t) = \begin{cases} x(t) = \int_0^t \sin\left(\frac{\pi}{2}u^2\right) du, \\ y(t) = \int_0^t \cos\left(\frac{\pi}{2}u^2\right) du. \end{cases}$$

The control points \mathbf{P}_0 and \mathbf{P}_3 are chosen such as $\mathbf{P}_0 = \mathbf{C}_1(-2.2)$ and $\mathbf{P}_3 = \mathbf{C}_1(-1.6)$. The tangents at these points verify $\theta_0 \approx -1.91$ and $\theta_3 \approx 1.67$. By considering the interpolation point $\mathbf{D} = \mathbf{C}_1(-1.9)$, the difference between the clothoid and the obtained ATPH solution is not discernible with the naked eye, unlike the PH one (see Figure 16).

7.3 Lemniscate

Let us consider the lemniscate, defined by the parametric equations

$$\mathbf{C}_2(t) = \begin{cases} x(t) = a\sqrt{2} \frac{\cos t}{1 + \sin^2 t}, \\ y(t) = a\sqrt{2} \frac{\sin t \cos t}{1 + \sin^2 t}, \end{cases}$$

with $t \in [0, 2\pi]$, herein for $a = 1$. We perform two different interpolations. In Figure 17a, we consider a symmetric arc with $\mathbf{P}_0 = \mathbf{C}_2\left(\frac{7\pi}{6}\right)$, $\mathbf{P}_3 = \mathbf{C}_2\left(\frac{7\pi}{6}\right)$, $\theta_3 = -\theta_0 \approx 1.39$. Figure 17b shows the fitting of a non-symmetric arc with $\mathbf{P}_0 = \mathbf{C}_2\left(\frac{7\pi}{12}\right)$, $\mathbf{P}_3 = \mathbf{C}_2\left(\frac{13\pi}{12}\right)$, $\theta_0 \approx -1.89$ and $\theta_3 \approx 1.17$. Once again, we clearly see that the cubic-like ATPH curve is closer to the reference curve than the PH one.

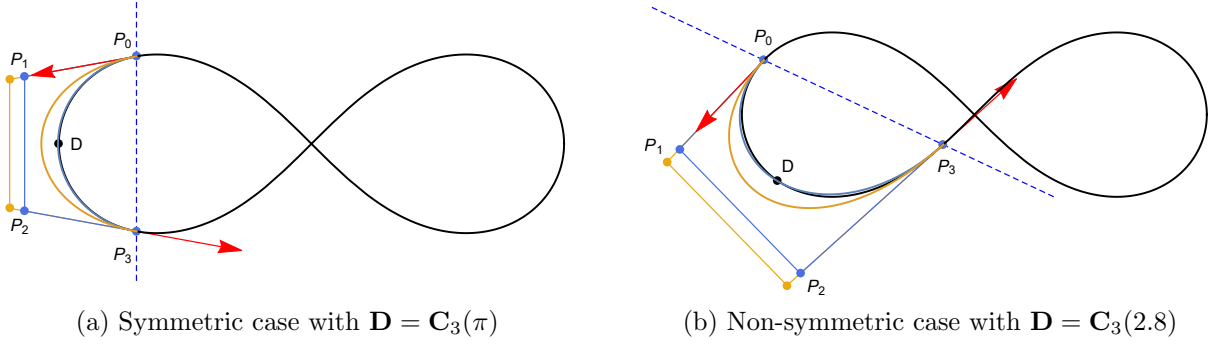


Figure 17: Interpolation of a lemniscate arc with a PH (orange) and an ATPH curves (blue).

7.4 Bernoullian quartic

Let us consider the Bernoullian quartic, defined by the parametric equations

$$\mathbf{C}_3(t) = \begin{cases} x(t) = \frac{(a^2 - b^2) \sin t \cos t}{\sqrt{a^2 \sin^2 t + b^2 \cos^2 t}} \\ y(t) = \frac{ab}{\sqrt{a^2 \sin^2 t + b^2 \cos^2 t}}, \end{cases}$$

with $t \in [0, \pi]$, herein for $a = 1$ and $b = 2$. We have $\mathbf{P}_0 = \mathbf{C}_3\left(\frac{5\pi}{6}\right)$, $\mathbf{P}_3 = \mathbf{C}_3\left(\frac{7\pi}{15}\right)$, then $\theta_0 \approx -2.07$ and $\theta_3 \approx 0.91$. Figure 18 illustrates three cases putting forward the position of \mathbf{D} on the shape of the interpolating curve. In Figure 18c, the quartic and ATPH curve are nearly overlapped.

8 Conclusion

In this paper, we have studied the construction process of a Hermite interpolation within the framework of the cubic-like ATPH. The domain Γ in which solutions exist has been rigorously described. Through the presence of the α parameter, the solution of the Hermite problem provided by ATPH curves is not unique. The analysis carried out between the parameter α and the control polygon allows us to understand its influence on the curve. This degree of freedom can be taken into account to solve additional problems. We have proposed an application through a fitting process illustrated by several examples.

Acknowledgments

The authors are grateful to the anonymous referees for their useful comments that helped to improve the clarity of the paper.

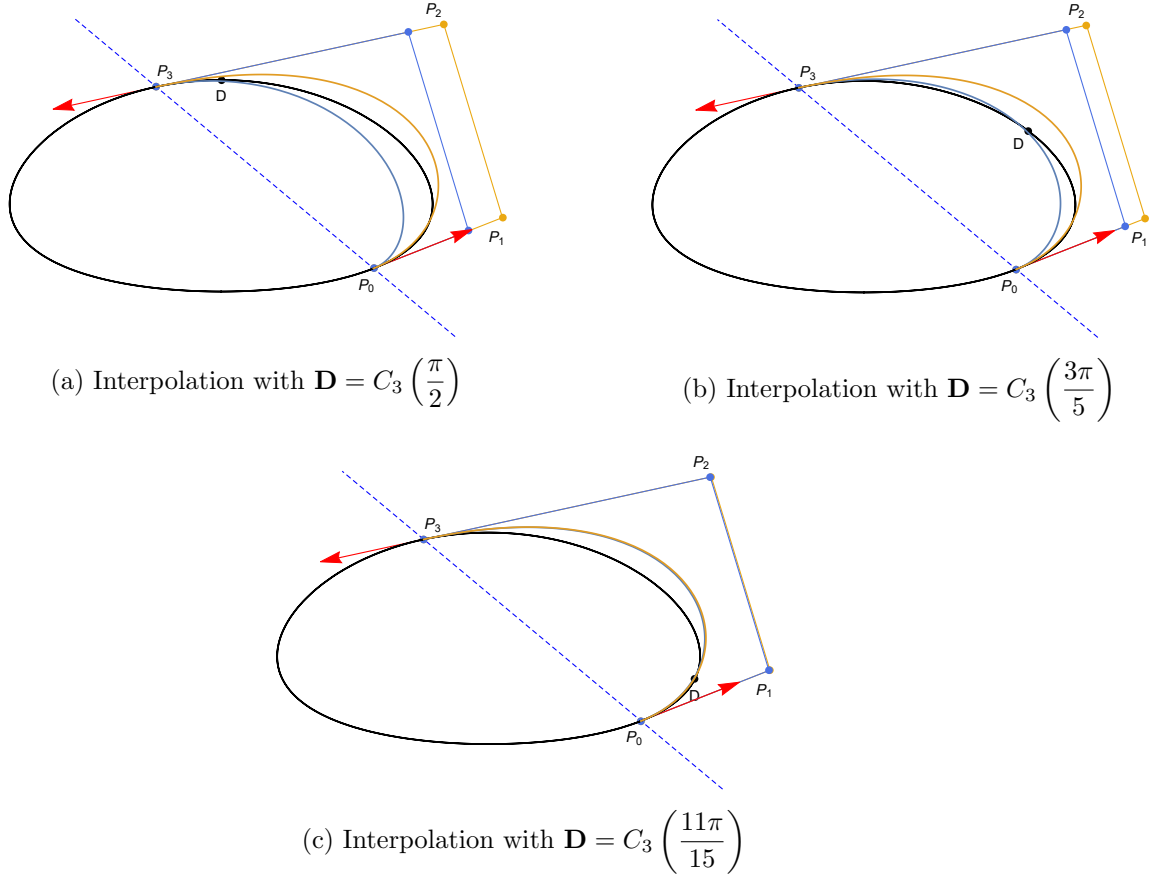


Figure 18: Interpolation of a Bernoullian quartic arc with the PH (orange) and the ATPH curves (blue).

References

- [1] B. Bastl, M. Bizzarri, M. Krajnc, M. Lávička, K. Slabá, Z. Šír, V. Vitrih, and E. Žagar. C^1 Hermite interpolation with spatial Pythagorean-hodograph cubic biarcs. Journal of Computational and Applied Mathematics, 257:65–78, 2014.
- [2] B. Bastl, K. Slabá, and M. Byrtus. Planar C^1 hermite interpolation with uniform and non-uniform TC-biarcs. Computer Aided Geometric Design, 30:58–77, 2013.
- [3] M. Byrtus and B. Bastl. G^1 Hermite interpolation by PH cubics revisited. Computer Aided Geometric Design, 27(8):622–630, 2010. Advances in Applied Geometry.
- [4] J.M. Carnicer and J.M. Peña. Totally positive bases for shape preserving curve design and optimality of B-splines. Computer Aided Geometric Design, 11(6):633–654, 1994.
- [5] I. Cattiaux. Normalized C-Basis and C-Curves. Wolfram Demonstration Project, 2015.
- [6] I. Cattiaux-Huillard and L. Saini. Characterization and extensive study of cubic and quintic algebraic trigonometric planar PH curves. Advances in Computational Mathematics, 46(2):28, 2020.
- [7] R. T. Farouki. The conformal map $z \rightarrow z^2$ of the hodograph plane. Computer Aided Geometric Design, 11(4):363–390, 1994.

- [8] R. T. Farouki, M. al Kandari, and T. Sakkalis. Hermite Interpolation by Rotation-Invariant Spatial Pythagorean-Hodograph Curves. Advances in Computational Mathematics, 17:369–383, 2002.
- [9] R. T. Farouki, C. Giannelli, C. Manni, and A. Sestini. Identification of spatial PH quintic Hermite interpolants with near-optimal shape measures. Computer Aided Geometric Design, 25:274–297, 2008.
- [10] R. T. Farouki and C. A. Neff. Hermite interpolation by pythagorean hodograph quintics. Mathematics of Computation, 64(212):1589–1609, 1995.
- [11] R. T. Farouki and T. Sakkalis. Pythagorean Hodographs. IBM Journal of Research and Development, 34:736–752, 1990.
- [12] M. Galetzka and P. Glauner. A Simple and Correct Even-Odd Algorithm for the Point-in-Polygon Problem for Complex Polygons. In 12th International Joint Conference on Computer Vision, Imaging and Computer Graphics Theory and Applications (VISIGRAPP 2017), pages 175–178, 2017.
- [13] B. Jüttler and C. Mäurer. Cubic pythagorean hodograph spline curves and applications to sweep surface modeling. Computer-Aided Design, 31:73–83, 1999.
- [14] E. Mainar, J. M. Peña, and J. Sánchez-Reyes. Shape preserving alternatives to the rational Bézier model. Computer Aided Geometric Design, 18(1):37–60, 2001.
- [15] D.S. Meek and D.J. Walton. Geometric Hermite interpolation with Tschirnhausen cubics. Journal of Computational and Applied Mathematics, 81(2):299–309, 1997.
- [16] H. P. Moon, R. T. Farouki, and H. I. Choi. Construction and shape analysis of PH quintic Hermite interpolants. Computer Aided Geometric Design, 18(2):93–115, 2001.
- [17] L. Romani and F. Montagner. Algebraic-Trigonometric Pythagorean-Hodograph Space Curves. Advances in Computational Mathematics, 45(1):75–98, 2019.
- [18] L. Romani, L. Saini, and G. Albrecht. Algebraic-Trigonometric Pythagorean-Hodograph curves and their use for Hermite interpolation. Advances in Computational Mathematics, 40(5-6):977–1010, 2014.
- [19] M. Shimrat. Algorithm 112: Position of Point Relative to Polygon. Communications of the ACM, 5(8):434, 1962.
- [20] W. Wu and X. Yang. Geometric Hermite interpolation by a family of spatial algebraic-trigonometric PH curves. Journal of Computational and Applied Mathematics, 388:113296, 2021.
- [21] S. Zbynek and B. Jüttler. C^2 Hermite interpolation by Pythagorean Hodograph space curves. Mathematics of Computation, 76:1373–1391, 2007.
- [22] J. Zhang. C-curves: An extension of cubic curves. Computer Aided Geometric Design, 13(3):199–217, 1996.
- [23] Z. Šír and B. Jüttler. C^2 hermite interpolation by pythagorean hodograph space curves. Mathematics of Computation, 76(259):1373–1391, 2007.

A Algorithm of the optimization process

Algorithm 1: Optimization with respect to α

Input: Point \mathbf{D} to fit, computational accuracy parameter η

Output: The optimized value of α

```
1  $\alpha_{max} \leftarrow 2\pi$ 
2  $\alpha_{min} \leftarrow 0$ 
3 if  $\theta_3 > \theta_0 + \frac{4}{3}\pi$  then
4    $\alpha_{min} \leftarrow \arg \min_{\alpha} |K_{\alpha} - 2 - 2 \cos(\theta_3 - \theta_0)|$ 
   // arg min stands for argument of the minimum, i.e. the elements of
   the domain at which the function value is minimized
5 end

   // Loop to reduce iteratively the research interval
6  $k \leftarrow 0$ 
7  $d_{err} \leftarrow E\left(\frac{\alpha_{min} + \alpha_{max}}{2}\right)$ 
8 while  $d_{err} > \eta$  do
9    $\alpha_k \leftarrow \frac{\alpha_{min} + \alpha_{max}}{2}$ 
10  Update the control points relating to  $\mathbf{r}_{\alpha_k}$ 
11  Compute hull of  $\mathbf{r}_{\alpha_k}$ 
12  if  $\mathbf{D} \in \text{hull of } \mathbf{r}_{\alpha_k}$  then
13     $\alpha_{min} \leftarrow \alpha_k$ 
14  else
15     $\alpha_{max} \leftarrow \alpha_k$ 
16  end
17   $d_{err} \leftarrow E(\alpha_k)$ 
18   $k \leftarrow k + 1$ 
19 end
20 return  $\alpha_k$ 
```
